

Electronic Supplementary Information

Elucidating the role of precursors in synthesizing single crystalline lithium niobate nanomaterials: A study of lithium precursors on nanoparticle quality

*Rana Faryad Ali, Byron D. Gates**

Department of Chemistry and 4D LABS, Simon Fraser University, 8888 University Drive
Burnaby, BC, V5A 1S6, Canada

* E-mail: bgates@sfu.ca

This work was supported in part by the Natural Sciences and Engineering Research Council of Canada (NSERC; Grant No. RGPIN-2020-06522), and through the Collaborative Health Research Projects (CHRP) Partnership Program supported in part by the Canadian Institutes of Health Research (Grant No. 134742) and the Natural Science Engineering Research Council of Canada (Grant No. CHRP 462260), the Canada Research Chairs Program (B.D. Gates, Grant No. 950-215846), CMC Microsystems (MNT Grant No. 6345), and a Graduate Fellowship (Rana Faryad Ali) from Simon Fraser University. This work made use of 4D LABS (www.4dlabs.com) and the Center for Soft Materials shared facilities supported by the Canada Foundation for Innovation (CFI), British Columbia Knowledge Development Fund (BCKDF), Western Economic Diversification Canada, and Simon Fraser University.

Experimental

Materials and supplies

All chemicals were of analytical grade and were used as received without further purification. Niobium ethoxide [$\text{Nb}(\text{OC}_2\text{H}_5)_5$, >90%] was obtained from Gelest Inc., and benzyl alcohol ($\text{C}_7\text{H}_7\text{OH}$, 99%) and triethylamine [$\text{N}(\text{C}_2\text{H}_5)_3$, 99.0%] were purchased from Acros Organics and Anachemia, respectively. Lithium chloride (LiCl , ~99.0%) was obtained from BDH Chemicals, and lithium bromide (LiBr , $\geq 99.0\%$), lithium fluoride (LiF , ~99.9%), and lithium iodide (LiI , 99.0%) were purchased from Sigma Aldrich. Lithium ethoxide (LiOC_2H_5 , 95.0%), lithium nitrate (LiNO_3 , $\geq 99.0\%$), lithium acetate (LiOOC_2H_3 , 98.0%), lithium carbonate (Li_2CO_3 , 99.9%), lithium sulfate (Li_2SO_4 , 99.9%), and a crystalline lithium niobate powder (LiNbO_3 , 99.9%, to serve as a reference material) were obtained from Sigma Aldrich. Lithium acetylacetonate [$\text{Li}(\text{acac})$, 99.5%], and lithium hydroxide monohydrate ($\text{LiOH}\cdot\text{H}_2\text{O}$, 99.0%) were purchased from Alfa Aesar. Anhydrous ethanol was obtained from Commercial Alcohols.

Synthesis of lithium niobate nanoparticles

Lithium niobate NPs were prepared in a single-step reaction using a previously reported solvothermal method.¹ In brief, 40 mM niobium ethoxide was dissolved in 10.0 mL of benzyl alcohol and stirred for 30 min, which resulted in the formation of a pale-yellow solution. This step was followed by the addition of 0.1 mL (i.e., 72 mM) of triethylamine and the mixture was stirred for another 30 min. After this period, a certain amount of each lithium precursor (selected from one of the reagents listed above) was added to the solution to produce a mixture containing a 1:1 mole ratio between Nb^{5+} and Li^+ . The solution was stirred for another 10 h at room temperature. The resulting mixture was transferred to a 23 mL Teflon lined autoclave (Model No. 4749, Parr

Instruments Co., Moline, IL, USA) and heated at 220 °C for 96 h. After cooling to room temperature, white precipitates were isolated from each solution via a process of centrifugation (Model No. AccuSpin 400, Fisher Scientific) at 8,000 rpm ($8,888 \times g$) for 20 min and decanting of the solution. These solids were washed three times by suspending the solids each time with 10 mL of ethanol and repeating the process of centrifugation and decanting of the solution. The purification process was also repeated three more times with 10 mL aliquots of deionized water (18 M Ω ·cm, produced using a Barnstead NANOpure DIamond water filtration system). The purified products were dried at 70 °C for 12 h to remove residual water prior to further analyses.

Characterization of lithium niobate nanoparticles

The morphology, dimensions, crystallinity, and lattice parameters of the LiNbO₃ NPs were characterized using an FEI Osiris X-FEG 8 transmission electron microscope (TEM) operated at an accelerating voltage of 200 kV. The TEM was calibrated using a thin film of aluminum before acquiring selected area electron diffraction (SAED) patterns from the samples. Samples for the TEM analyses were prepared by dispersing the purified products in ethanol followed by drop-casting 5 μ L of each suspension onto a separate TEM grid (200 mesh copper grids coated with Formvar/carbon) purchased from Cedarlane Laboratories. Each TEM grid was dried at \sim 230 Torr for at least 20 min prior to analysis. The TEM apertures used to acquire the SAED patterns from multiple NPs were 40 μ m and 200 μ m.

Phase and crystallinity of the samples were further determined from X-ray diffraction (XRD) patterns acquired with a Rigaku R-Axis Rapid diffractometer equipped with a 3 kW sealed tube copper source ($K\alpha$ radiation, $\lambda = 0.15418$ nm) collimated to 0.5 mm. Powder samples were

packed into a cylindrical recess drilled into a glass microscope slide (Leica 1 mm Surgipath Snowcoat X-tra Micro Slides) for acquiring XRD patterns of the products.

Purity and phase of the product with respect to the desired rhombohedral phase were further assessed using Raman spectroscopy techniques. Raman spectra were collected using a Renishaw inVia Raman microscope with a 50× objective lens (Leica, 0.5 NA) and a 514 nm laser (argon-ion laser, Model No. Stellar-Pro 514/50) set to 100% laser power with an exposure time of 60 s. The Raman spectrometer was calibrated by collecting the Raman spectrum of a polished silicon (Si) standard with a distinct peak centered at 520 cm^{-1} . The Raman spectra for the samples were acquired from 100 to 1,000 cm^{-1} using a 1,800 lines/mm grating.

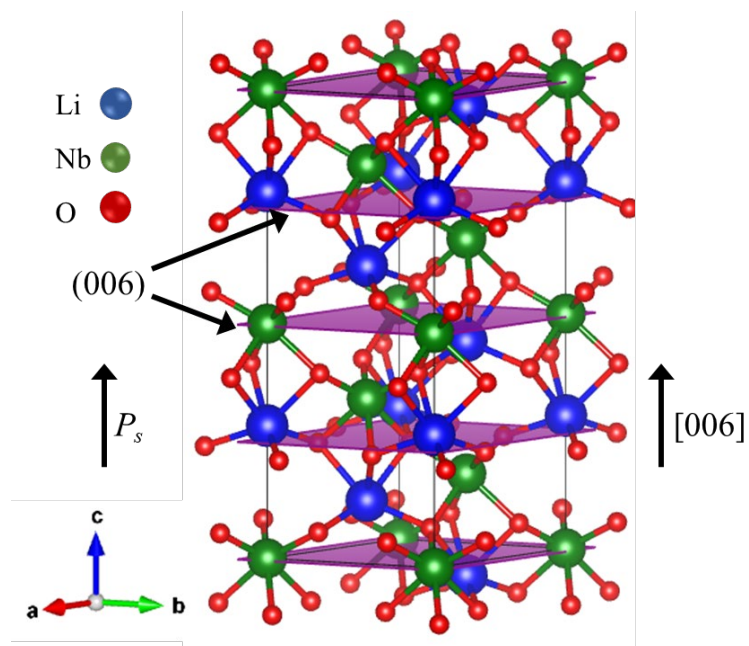


Fig. S1 Crystal structure of the lithium niobate (LiNbO₃) depicting its growth along the $[006]$ direction, which corresponds to the direction of spontaneous polarization (P_s) of the LiNbO₃ lattice.

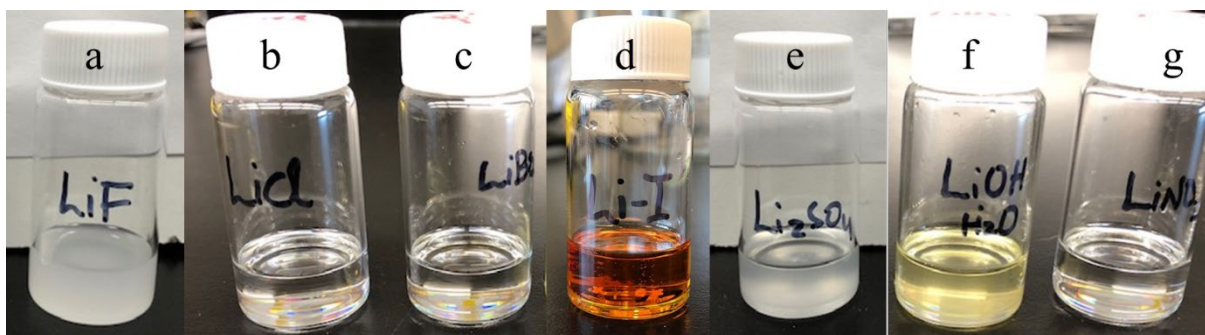


Fig. S2 Image depicting the benzyl alcohol solubility of a series of the lithium (Li) precursors with non-carbon-based anionic species: (a) lithium fluoride (LiF); (b) lithium chloride (LiCl); (c) lithium bromide (LiBr); (d) lithium iodide (LiI); (e) lithium sulfate (Li₂SO₄); (f) lithium hydroxide monohydrate (LiOH·H₂O); and (g) lithium nitrate (LiNO₃). Each of these precursors exhibited a good solubility in the benzyl alcohol, yielding relatively clear solutions except for LiF and Li₂SO₄. The color of solution containing the LiI precursor turned brown, which indicated the formation of triiodide in the benzyl alcohol.

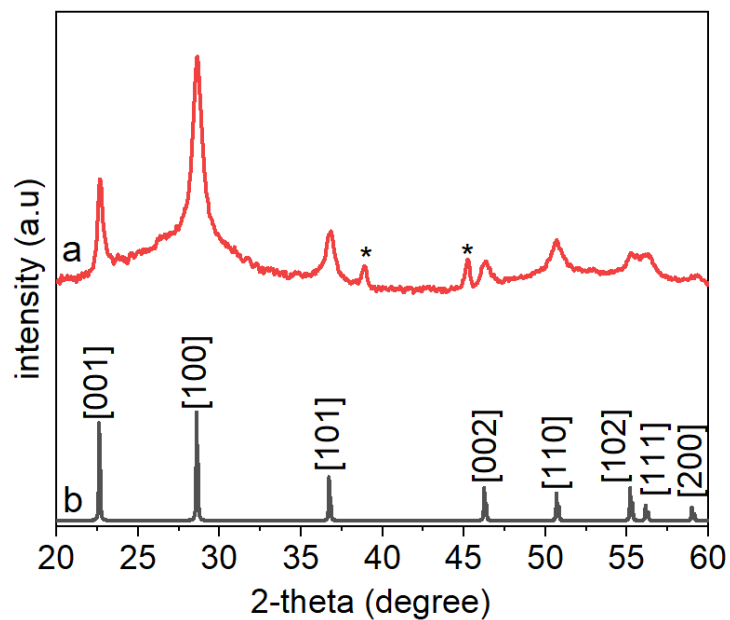


Fig. S3 Powder X-ray diffraction patterns for: (a) niobium oxide (Nb_2O_5) nanowires prepared using LiF as one of the precursors in the described solution-phase synthesis that evaluated various precursors on the ability to prepare LiNbO_3 particles; and (b) a reported Nb_2O_5 reference (JCPDS No. 028-0317). The presence of a LiF impurity in the products is indicated by (*).

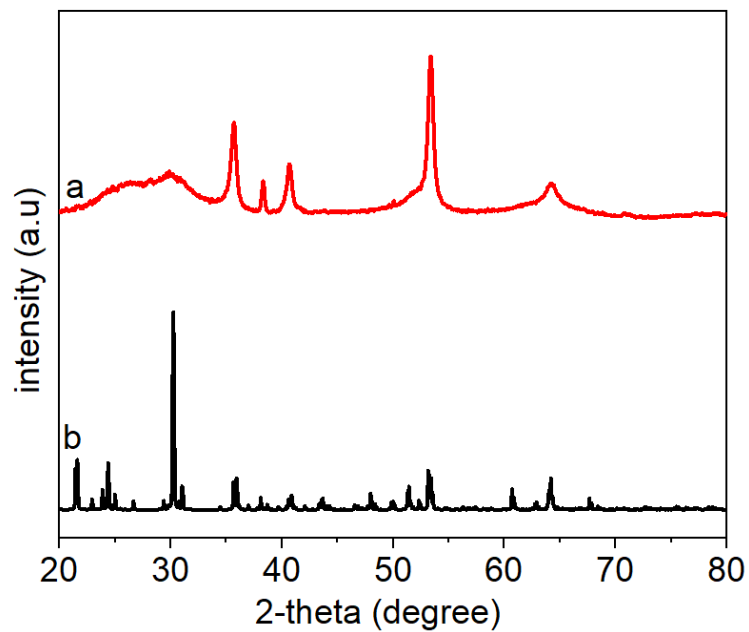


Fig. S4 Powder X-ray diffraction patterns for: (a) products prepared using LiI as one of the precursors in the described solution-phase synthesis that evaluated various precursors on the ability to prepare LiNbO_3 particles; and (b) a reported LiNb_3O_8 reference (JCPDS No. 011-2140).

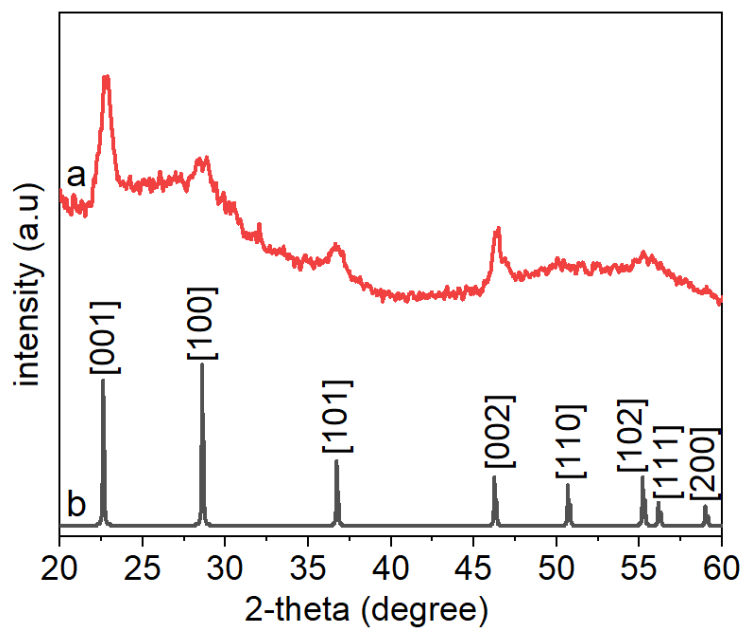


Fig. S5 Powder X-ray diffraction patterns for: (a) Nb_2O_5 nanowires prepared using Li_2SO_4 as one of the precursors in the described solution-phase synthesis that evaluated various precursors on the ability to prepare LiNbO_3 particles; and (b) a reported Nb_2O_5 reference (JCPDS No. 028-0317).

Table S1. Average dimensions of LiNbO₃ nanoparticles prepared using lithium precursors with non-carbon-based anionic species.

lithium precursor	mean particle size* (nm)	average size of crystallite ‡ (nm) [012]	average size of crystallite ‡ (nm) [104]	average size of crystallite ‡ (nm) [110]	average size of crystallite ‡ (nm) [116]
LiCl	48 ± 10	25.2	25.7	8.5	20.7
LiBr	43 ± 11	24.1	23.7	13.9	14.7
LiOH·H ₂ O	91 ± 18	25.2	20.3	22.4	15.7
LiNO ₃	44 ± 12	22.2	21.5	9.7	19.6

* Results prepared from TEM analyses (e.g., see Fig. 3 for further details).

‡ Results prepared using Scherrer analyses of the peak widths for the [012], [104], [110], and [116] reflections of the corresponding X-ray diffraction (XRD) patterns (Fig. 2).

Table S2. Peak area ratios as measured from specific XRD reflections for a LiNbO₃ reference material and for the LiNbO₃ nanoparticles prepared using the specific Li precursors indicated above each column.

XRD peak ratios	LiNbO ₃ [‡] (JCPDS No. 020-0631)	LiCl	LiBr	LiOH·H ₂ O	LiNO ₃
(104)/(012)	0.37	0.62	0.32	0.44	0.56
(110)/(012)	0.22	1.02	1.95	0.26	0.63
(024)/(012)	0.17	0.41	0.20	0.20	0.34
(116)/(012)	0.25	1.59	3.84	0.34	0.99

[‡] Reference material included for comparative purposes.

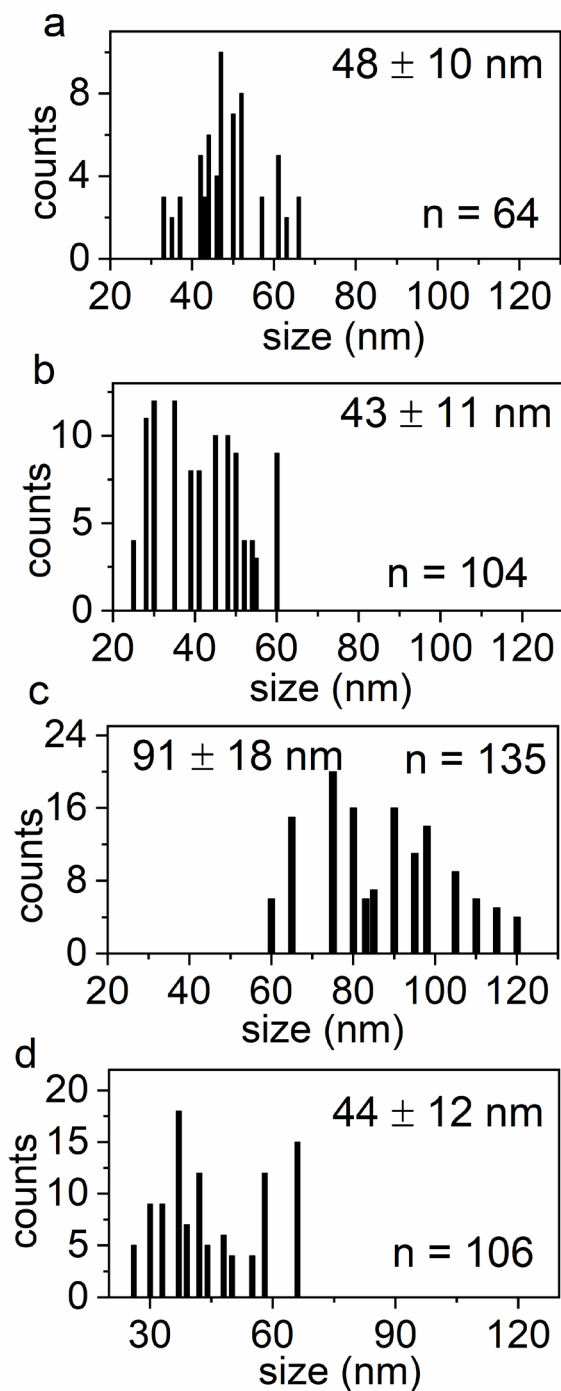


Fig. S6 Histograms showing the dimensions of lithium niobate (LiNbO_3) nanoparticles synthesized using: (a) LiCl ; (b) LiBr ; (c) $\text{LiOH}\cdot\text{H}_2\text{O}$; or (d) LiNO_3 as the Li precursor. The mean particle diameter and one standard deviation from the calculated mean value are reported on each histogram. These measurements were obtained from the analysis of transmission electron microscopy (TEM) data obtained for each product. The total number of nanoparticles measured for each dataset (n) are reported on their respective histograms.

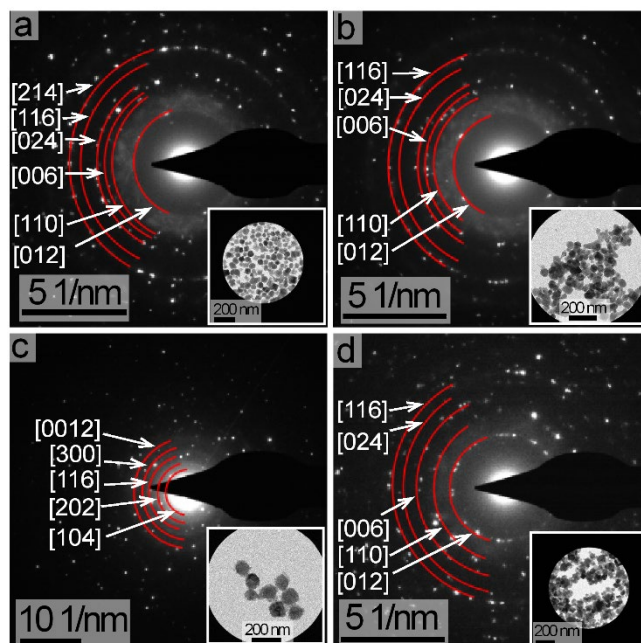


Fig. S7 Analyses by selected area electron diffraction (SAED) of LiNbO_3 nanoparticles obtained using: (a) LiCl ; (b) LiBr ; (c) $\text{LiOH}\cdot\text{H}_2\text{O}$; or (d) LiNO_3 . Inset images portray the collection of nanoparticles analyzed for each sample as viewed by TEM.

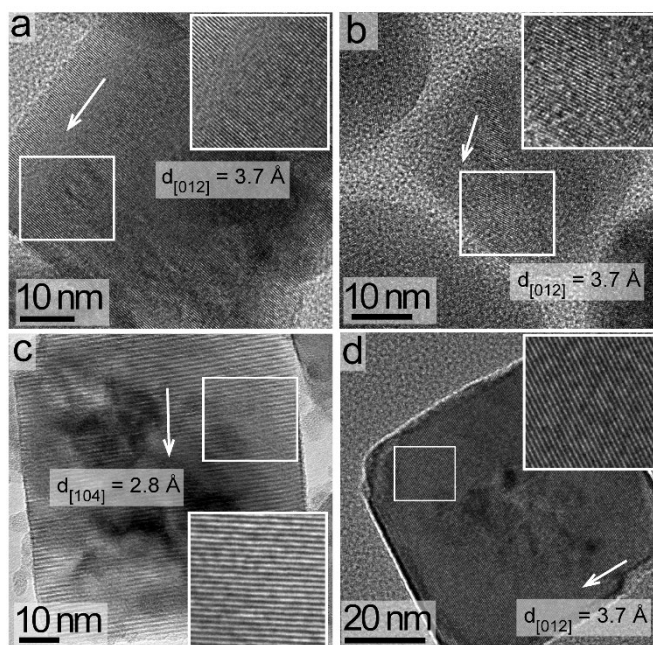


Fig. S8 Representative high resolution TEM (HRTEM) analyses of LiNbO₃ nanoparticles obtained using: (a) LiCl; (b) LiBr; (c) LiOH·H₂O; or (d) LiNO₃. The insets portray a higher magnification of each sample obtained from the regions indicated by the white boxes. The white arrows depict the direction of the observed fringe patterns, whose d-spacing is assigned on each image.

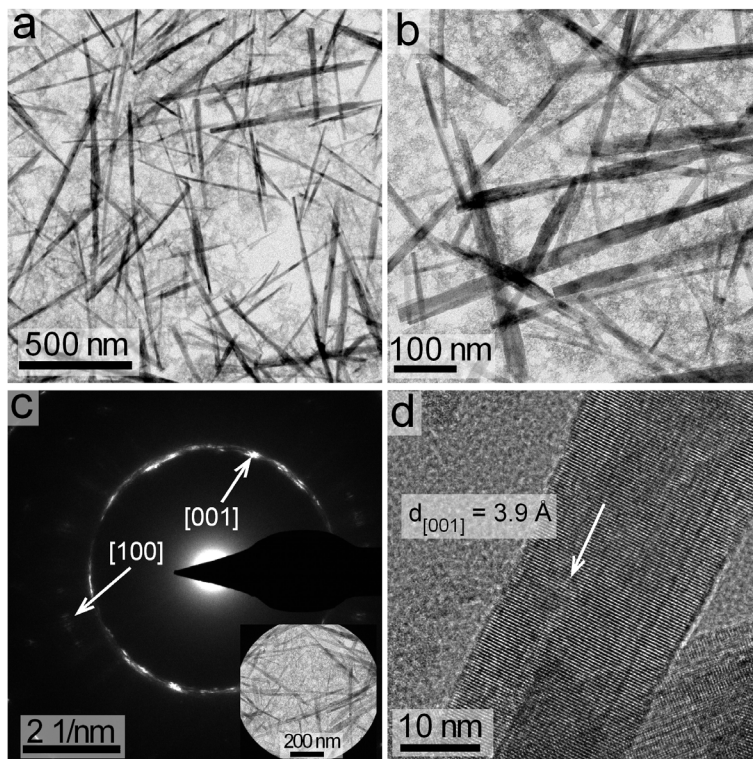


Fig. S9 Products synthesized by a solvothermal method using LiF as a precursor, which were characterized by: (a and b) TEM; (c) SAED; and (d) HRTEM analyses.

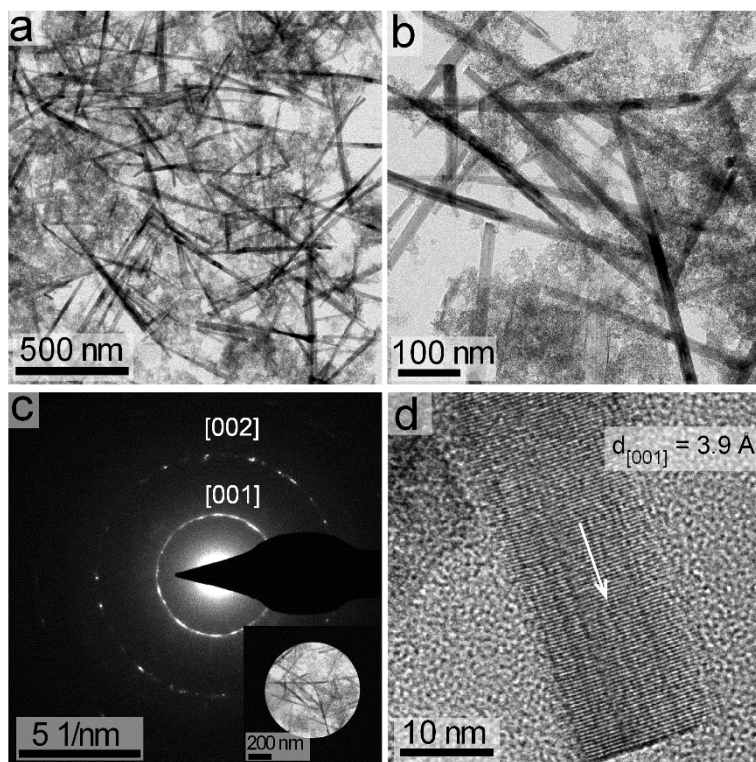


Fig. S10 Products synthesized by a solvothermal method using Li_2SO_4 as a precursor, which were characterized by: (a and b) TEM; (c) SAED; and (d) HRTEM analyses.

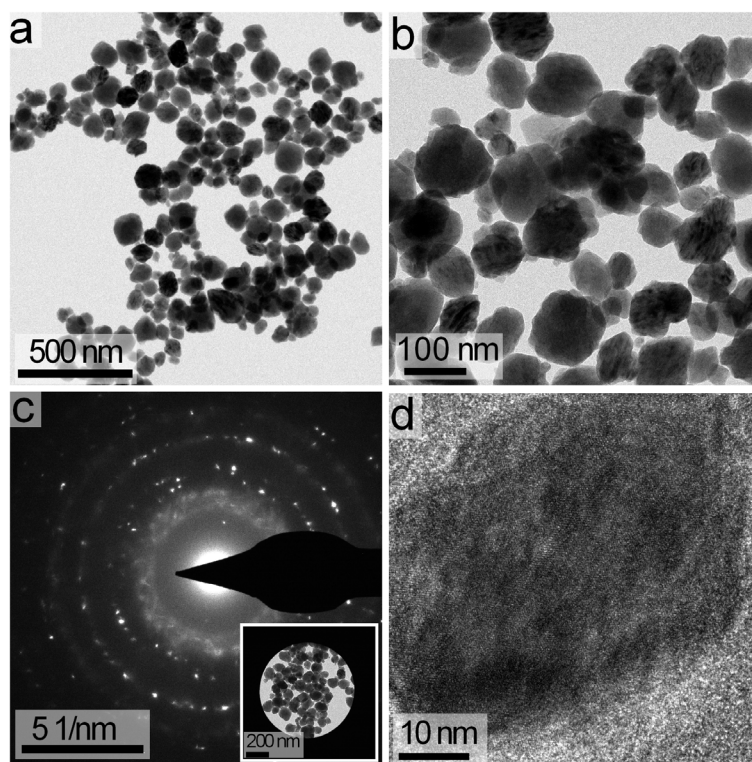


Fig. S11 Products synthesized by a solvothermal method using LiI as a precursor, which were characterized by: (a and b) TEM; (c) SAED; and (d) HRTEM analyses.

Table S3. Bond vibrations associated with the Raman spectral bands of LiNbO₃.¹

wavenumber (cm ⁻¹)	vibrations
~150	Nb-O vibrations
~260	δ (Li-O + LiO ₆)
~225 and ~334	NbO ₆ deformations
~375 and ~430	δ (Nb-O-Nb)
~620	ν _s (NbO ₆)
~870	ν _{as} (Nb-O-Nb)
~900	ν (Nb=O)

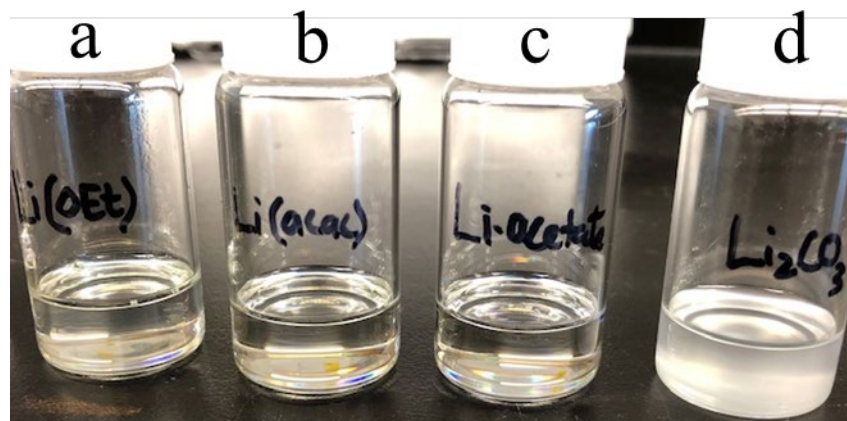


Fig. S12 Image depicting the benzyl alcohol solubility of a series of Li precursors containing carbon-based anionic species: (a) lithium ethoxide [$\text{Li}(\text{OC}_2\text{H}_5)$]; (b) lithium acetylacetonate [$\text{Li}(\text{acac})$]; (c) lithium acetate [$\text{Li}(\text{OOC}_2\text{H}_3)$]; and (d) lithium carbonate (Li_2CO_3). Each of these precursors exhibited a good solubility in benzyl alcohol except for the Li_2CO_3 , which yielded white precipitates due to its relatively poor solubility in the solvent.

Table S4. Average dimensions of LiNbO₃ nanoparticles prepared using Li precursors containing carbon-based anionic species.

lithium precursor	mean particle size*	average size of crystallite ‡	average size of crystallite ‡	average size of crystallite ‡	average size of crystallite ‡
	(nm)	(nm) [012]	(nm) [104]	(nm) [110]	(nm) [116]
Li(OC ₂ H ₅)	48 ± 9	23.4	22.0	23.5	18.1
Li(acac)	31 ± 7	11.9	12.7	15.6	28.7
Li(OOC ₂ H ₃)	390 ± 54	23.1	24.7	11.8	22.3
Li ₂ CO ₃	827 ± 147	26.1	26.6	25.4	22.0

* Results prepared from TEM analyses (e.g., see Fig. 6 for further details).

‡ Results prepared using Scherrer analyses of the peak widths for the [012], [104], [110], and [116] reflections of the corresponding XRD patterns (Fig. 5).

Table S5. Peak area ratios as measured from specific XRD reflections for a LiNbO₃ reference material and for the LiNbO₃ nanoparticles prepared using the specific Li precursors indicated above each column.

XRD peak ratios	LiNbO ₃ [‡] (JCPDS No. 020-0631)	Li(OC ₂ H ₅)	Li(acac)	Li(OOC ₂ H ₃)	Li ₂ CO ₃
(104)/(012)	0.37	0.58	0.47	0.84	0.55
(110)/(012)	0.22	0.35	0.37	1.27	0.62
(024)/(012)	0.17	0.37	0.23	0.50	0.35
(116)/(012)	0.25	0.56	0.53	2.23	0.83

[‡] Reference material included for comparative purposes.

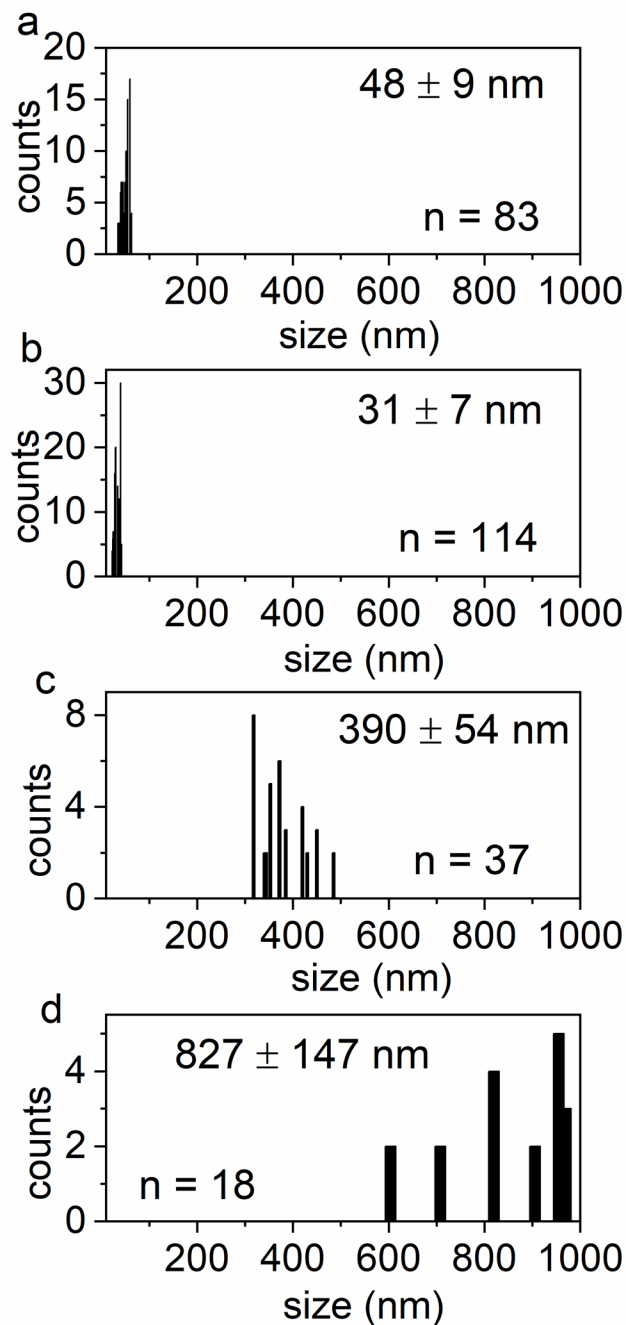


Fig. S13 Histograms showing the dimensions of LiNbO_3 nanoparticles synthesized using: (a) $\text{Li}(\text{OC}_2\text{H}_5)$; (b) $\text{Li}(\text{acac})$; (c) $\text{Li}(\text{OOC}_2\text{H}_3)$; or (d) Li_2CO_3 as the Li precursor. The mean particle diameter and one standard deviation from the calculated mean value are reported on each histogram. These measurements were obtained from the analyses of TEM data obtained for each product. The total number of nanoparticles measured for each type of sample (n) are reported on each of the corresponding histograms.

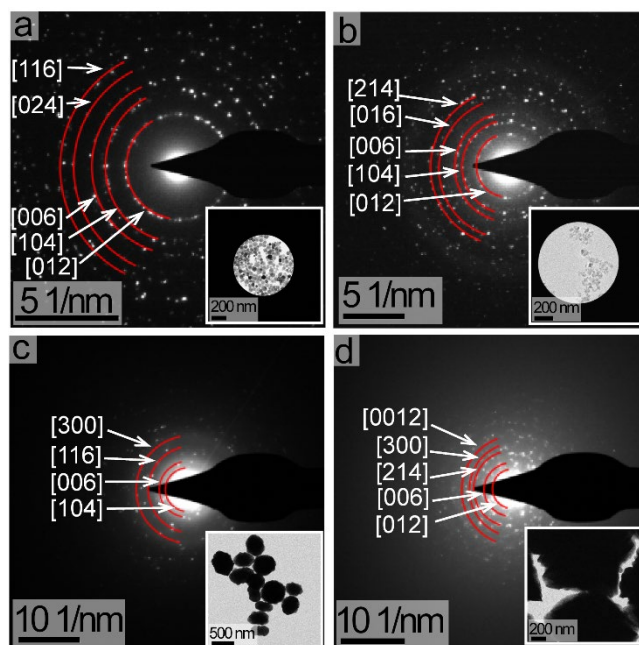


Fig. S14 The SAED analyses of LiNbO_3 nanoparticles synthesized using: (a) $\text{Li}(\text{OC}_2\text{H}_5)$; (b) $\text{Li}(\text{acac})$; (c) $\text{Li}(\text{OOC}_2\text{H}_3)$; or (d) Li_2CO_3 as the Li precursor. Inset images portray the collection of nanoparticles analyzed for each sample as viewed by TEM.

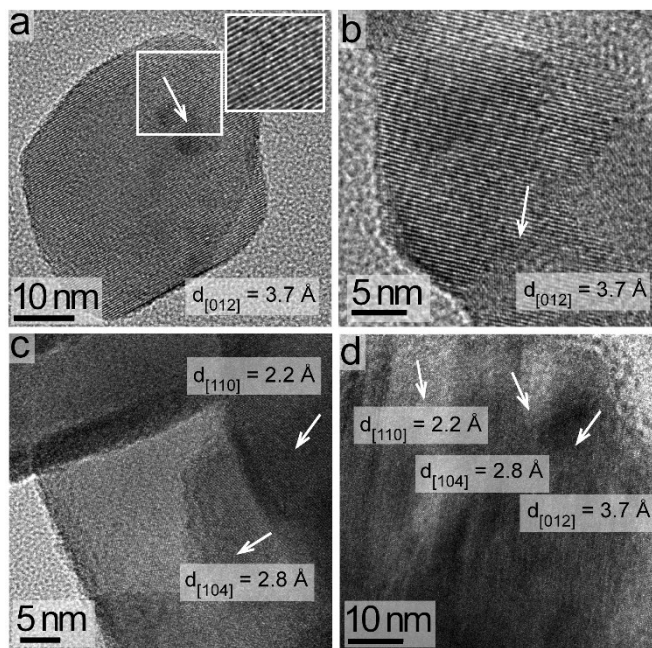


Fig. S15 Representative HRTEM analyses of LiNbO_3 nanoparticles prepared using: (a) $\text{Li}(\text{OC}_2\text{H}_5)$; (b) $\text{Li}(\text{acac})$; (c) $\text{Li}(\text{OOC}_2\text{H}_3)$; or (d) Li_2CO_3 . The inset in (a) portrays a higher magnification of the sample from the region indicated by the white box. The white arrows depict the directions of the observed fringe patterns, whose d-spacing is assigned upon each image.

Table S6. A sample of additional materials prepared from different lithium precursors. The selection of lithium precursor also plays a crucial role in determining the crystallinity, purity, and aggregation of these products.

Titles of the Corresponding Manuscript	Alkali Metal Precursors Used	Products	Reference
Structural Evolution and Formation Mechanism of LiNiO ₂ During High-Temperature Solid State Synthesis	Li ₂ CO ₃ LiOH	LiNiO ₂	2
<i>In Situ</i> XRD Studies During Synthesis of Single-Crystal LiNiO ₂ , LiNi _{0.975} Mg _{0.025} O ₂ , and LiNi _{0.95} Al _{0.05} O ₂ Cathode Materials	Li ₂ CO ₃ LiOH	LiNiO ₂ LiNi _{0.975} Mg _{0.025} O ₂ LiNi _{0.95} Al _{0.05} O ₂	3
Low-Temperature Synthesis of LiCoO ₂ with Eutectic of Lithium Precursors via the Solid-State Reaction Method	LiOH·H ₂ O Li ₂ CO ₃	LiCoO ₂	4
Lithium-Metal Oxide Nanoparticles, Preparation Method and Use Thereof	LiOH·H ₂ O Li ₂ CO ₃ LiNO ₃ Li ₂ SO ₄	xLi ₂ MnO ₃ (1-x)LiNi _y Co _z Mn _{1-y-z} O ₂ where 0<x<1 0<y<1, 0<z<1	5
Stabilizing Li-Rich NMC Materials by Using Precursor Salts with Acetate and Nitrate Anions for Li-Ion Batteries	LiC ₂ H ₃ O ₂ LiNO ₃	Li _{1.2} Mn _{0.5100} Ni _{0.2175} Co _{0.0725} O ₂	6
Method for Preparing Lithium Iron Phosphate Nanopowder	Li(OOC ₂ H ₃)·2H ₂ O LiOH·H ₂ O LiOH, Li ₂ CO ₃	LiFePO ₄	7
Method for Making Lithium Iron Phosphate	LiOH, LiCl Li ₂ SO ₄ , LiNO ₃ LiH ₂ PO ₄ Li(OOC ₂ H ₃)	LiFePO ₄	8
Solution Based Synthesis of Mixed-Phase Materials in the Li ₂ TiO ₃ -Li ₄ SiO ₄ System.	LiCl, Li ₂ CO ₃ LiNO ₃ , Li ₂ SO ₄ Li(OOC ₂ H ₃)	Li ₂ TiO ₃ Li ₄ SiO ₄	9
Effect of Added Potassium Salt on Preparation of Potassium Niobate by Hydrothermal Processing	KCl, K ₂ SO ₄ K ₂ CO ₃ KBr, KOH	KNbO ₃	10

References

- [1] R. F. Ali and B. D. Gates, *Chem. Mater.*, 2018, **30**, 2028–2035.
- [2] S. Deng, L. Xue, Y. Li, Z. Lin, W. Li, Y. Chen, T. Lei, J. Zhu and J. Zhang, *J. Electrochem. Energy Convers. Storage*, 2019, **16**, 031004.
- [3] R. Weber, H. Li, W. Chen, C.-Y. Kim, K. Plucknett and J. R. Dahn, *J. Electrochem. Soc.*, 2020, **167**, 100501.
- [4] R. Liang, S. Yonezawa, J.-H. Kim and T. Inoue, *J. Asian Ceram. Soc.*, 2018, **6**, 332–341.
- [5] Y. Xia, 2015, U.S. Patent Application No. 14/367,578.
- [6] K. I. Hamad and Y. Xing, *Batteries*, 2019, **5**, 69.
- [7] I. K. Jun, S. B. Cho and M. H. Oh, 2017, U.S. Patent No. 9,755,234.
- [8] L. Wang, X.-M. He, J.-X. Wang, J. Gao and J.-J. Li, 2017, U.S. Patent No. 9,822,014.
- [9] D. A. H. Hanaor, M. H. H. Kolb, Y. Gan, M. Kamlah and R. Knitter, *J. Nucl. Mater.*, 2015, **456**, 151–161.
- [10] C. Bao, Y. Jie, Y. Bin, Z. Xinpeng, Y. Cheng, C. Junwen, C. Huiqun, *Chinese Journal of Lasers*, 2013, **40**, 806005.